JOURNAL OF SOLID STATE CHEMISTRY **122,** 384–389 (1996)
ARTICLE NO. 0131

# Electron Paramagnetic Resonance Spectra of $Pr^{4+}$ in $BaCeO_3$, $BaZrO_3$, $BaSnO_3$, and Their Solid Solutions

Yukio Hinatsu

*Department of Chemistry, Faculty of Science, Hokkaido University, Kita-ku, Sapporo 060, Japan*

Received August 7, 1995; in revised form January 3, 1996; accepted January 5, 1996

**The electron paramagnetic resonance (EPR) spectra of powders with $Pr^{4+}$ doped in $BaCeO_3$, $BaZrO_3$, $BaSnO_3$, and their solid solutions were measured at 4.2 K. A very large hyperfine interaction with the $^{141}Pr$ nucleus was observed. The results were analyzed based on the weak field approximation, i.e., the Breit–Rabi formula, and the $g$ values and hyperfine coupling constants $A$ were obtained. The measured $g$ values are much smaller than $|-1.429|$, which shows that the crystal field effect on the behavior of a $4f$ electron is large. The value of $|g|$ decreases from 0.741 ($Pr^{4+}/BaCeO_3$) to 0.583 ($Pr^{4+}/BaSnO_3$), and is caused by the increase of the crystal field due to the shrinking of the lattice. On the other hand, the hyperfine coupling constants are almost constant: $A = 0.060(1)$ cm$^{-1}$.** 

## INTRODUCTION

The electronic configuration of the tetravalent praseodymium ion is $[Xe]4f^1$. For electronic structure analysis, this $f^1$ configuration is straightforward, as only the crystal field and spin-orbit coupling interactions are important. Especially when this ion is located in an octahedral crystal field environment, such a compound is suitable to study the behavior of a $4f$ electron in solids because it is easy to compare the experimental results with theoretical calculations.

Although the trivalent oxidation state of praseodymium is most stable, the tetravalent state is accessible (1). Perovskite-type oxides, $ABO_3$, where $A$ is a divalent ion (e.g., Sr, Ba) accommodate tetravalent metal ions at the $B$ site of the crystal (2). Figure 1 shows the crystal structure of cubic perovskite $ABO_3$.

In an earlier study (3), we had successfully measured for the first time the EPR spectrum of the $Pr^{4+}$ ion in an octahedral crystal field by doping it in the perovskite $BaCeO_3$ (where the $Pr^{4+}$ ion is substituted for the $Ce^{4+}$ ion) and lowering the experimental temperature to liquid helium temperatures. In the EPR spectrum, a very large hyperfine interaction with the $^{141}Pr$ nucleus (nuclear spin $I = 5/2$) was measured. In addition to the allowed hyperfine interactions, forbidden hyperfine transitions were observed.

Although the crystal structure of $BaCeO_3$ is an orthorhombically distorted perovskite, the distortion from the ideal cubic perovskite structure ($\beta \simeq 90°$) is very small; i.e., the oxygen coordination around the central $Pr^{4+}$ in the host material has nearly octahedral symmetry, and the EPR results could be analyzed based on the weak field approximation (i.e., Breit–Rabi formula) with an octahedral crystal field around $Pr^{4+}$. The results show that, although this is a $4f$ electron system, the crystal field influences the magnetic properties of a $4f$ electron (3). However, the effect of the crystal field strength on the behavior of a $4f$ electron in solids is still unclear.

In this study, we have prepared samples in which $Pr^{4+}$ ions are doped in cubic $BaSnO_3$, $BaZrO_3$, $BaCeO_3$, and their solid solutions and measured their electron paramagnetic resonance spectra. The effect of the crystal field on the behavior of a $4f$ electron is discussed.

## EXPERIMENTAL

### 1. Sample Preparation

$BaCO_3$, $Pr_6O_{11}$, and $CeO_2$ (and/or $ZrO_2$, $SnO_2$) were used as the starting materials. Before use, the $Pr_6O_{11}$ was reduced to the stoichiometric $Pr_2O_3$ by heating it in a flow of hydrogen gas at 1000°C for 8 hr. The $CeO_2$, $ZrO_2$, and $SnO_2$ were heated in air at 850°C to remove any moisture and oxidized to the stoichiometric compositions. They were weighed in the correct metal ratios $BaPr_{0.02}M_{0.98}O_3$ ($M$ = Ce, Zr, Sn), intimately mixed, and heated in a flowing oxygen atmosphere at 1300°C in an SiC resistance furnace for a day. The samples $BaPr_{0.05}Zr_{0.95}O_3$ and $BaPr_{0.05}Sn_{0.95}O_3$ were also prepared. After cooling to room temperature, the samples were crushed into powder, reground, repressed into pellets, and heated under the same conditions to make the reaction complete.

### 2. Analysis

An X-ray diffraction analysis was performed with Cu$K\alpha$ radiation on a Philips PW 1390 diffractometer equipped with a curved graphite monochromator. The samples pre-



0022-4596/96 $18.00

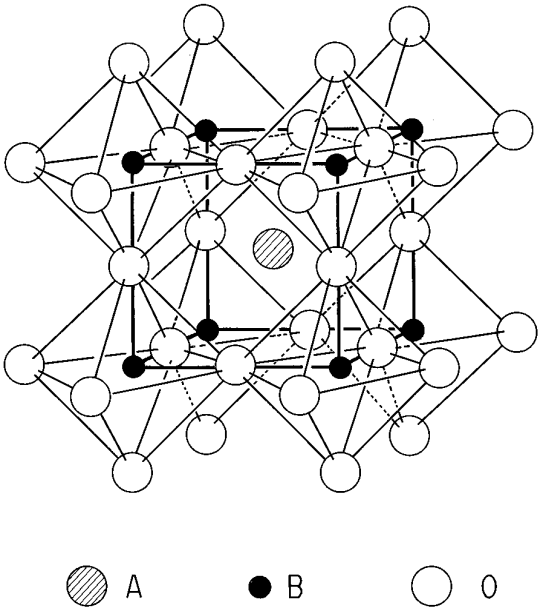


**FIG. 1.** Crystal structure of cubic perovskite $ABO_3$.

pared in this study were formed in single phase with the perovskite-type structure and their lattice parameters are given in the second column of Table 3.

*3. Electron Paramagnetic Resonance Measurement*

The EPR spectra at X band (9.093 GHz) were measured using a JEOL RE-2X spectrometer operating with an Air Products Helitran cooling system. The magnetic field was swept from 100 to 13,500 G. Before the samples were measured, a blank was recorded to eliminate the possibility of interference by the background resonance of the cavity and/or the sample tube. The magnetic field was monitored with a proton NMR gaussmeter, and the microwave frequency was measured with a frequency counter.

## RESULTS AND DISCUSSION

The EPR spectra for $Pr^{4+}$ could be measured at 4.2 K in all the host materials. With increasing temperature, all the assigned absorption EPR lines became considerably weaker in intensity. This observation strongly indicates that the oxidation state of the praseodymium ion is not trivalent, but tetravalent, because the non-Kramers $Pr^{3+}$ ion usually shows no EPR spectrum (4).

Figure 2 shows the EPR spectra for $Pr^{4+}$ doped in $BaCeO_3$ and $BaCe_{0.90}Zr_{0.10}O_3$ measured at 4.2 K. The observed spectra are complicated and composed of many absorption lines. We have analyzed the spectrum for the case of $Pr^{4+}/BaCeO_3$ (3). Six absorption lines due to allowed transitions are observed, along with five weaker absorption lines due to forbidden transitions (one of which overlaps with an allowed transition). In the host materials, $BaCe_{1-y}Zr_yO_3$ ($y > 0.1$), $BaZrO_3$, $BaZr_{1-y}Sn_yO_3$, and $BaSnO_3$, no EPR absorption lines due to forbidden transitions are observed. This is due to the fact that since the EPR spectra for $Pr^{4+}$ became broader with increasing Zr content in the $BaCe_{1-y}Zr_yO_3$ and in the other host materials, the absorption lines due to the forbidden transitions are hidden in the background levels. Figure 3 shows the EPR spectra for $BaPr_{0.02}Zr_{0.98}O_3$ and $BaPr_{0.02}Sn_{0.98}O_3$ measured at 4.2 K.

The tetravalent praseodymium $Pr^{4+}$ is a Kramers' ion with one unpaired $4f$ electron and in a magnetic field one isotropic EPR spectrum may be observable. The isotope $^{141}Pr$ (natural abundance 100%) has a nuclear spin of $I = 5/2$ and a nuclear magnetic moment of $+4.3\ \mu_N$. The spin Hamiltonian for the EPR spectrum of $Pr^{4+}/BaMO_3$ ($M$ = Ce, Zr, Sn) is

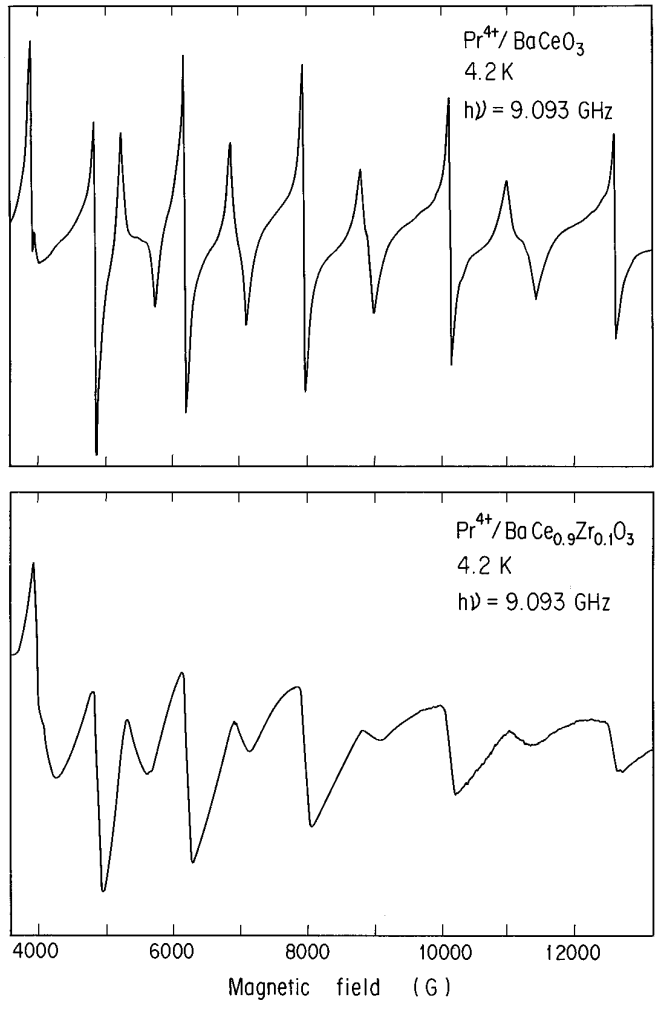


**FIG. 2.** EPR spectra for $Pr^{4+}$ doped in $BaCeO_3$ and in $BaCe_{0.90}Zr_{0.10}O_3$ measured in 4.2 K.

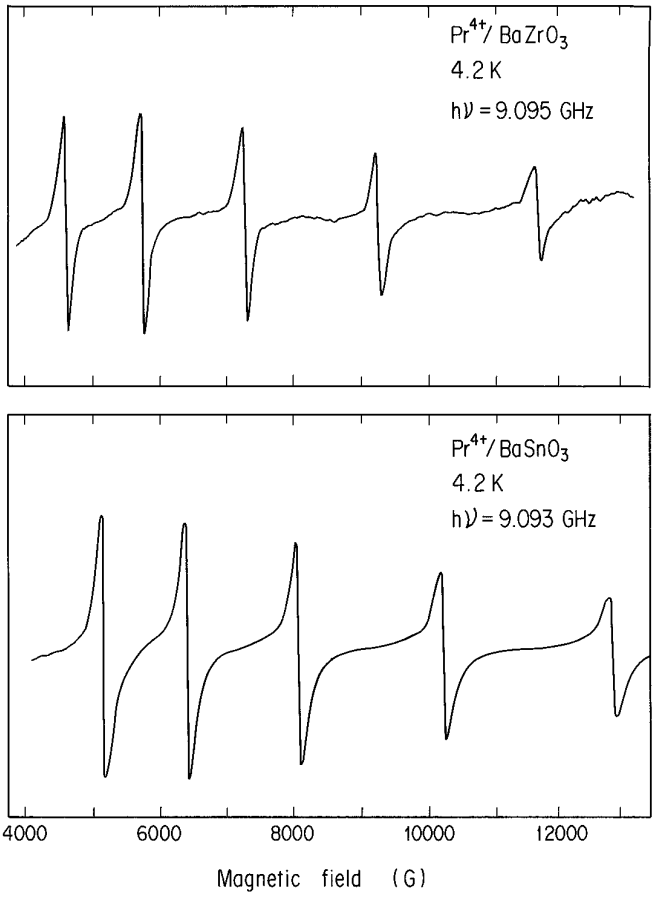


**FIG. 3.** EPR spectra for $BaPr_{0.02}Zr_{0.98}O_3$ and $BaPr_{0.02}Sn_{0.98}O_3$ at 4.2 K.

$$\mathcal{H} = g\beta\mathbf{H}\cdot\mathbf{S}' + A\mathbf{I}\cdot\mathbf{S}' - g'_N\beta\mathbf{H}\cdot\mathbf{I}, \qquad [1]$$

where $g$ is the $g$ value for the $Pr^{4+}$ with an effective spin $\mathbf{S}' = 1/2$, $A$ is the hyperfine coupling constant, $g'_N$ is the effective nuclear $g$ value (in units of $\mu_B$), $\beta$ is the Bohr magneton, and $\mathbf{H}$ is the applied magnetic field. Usually the assumption can be made that the electronic Zeeman term (the first term on the right-hand side of Eq. [1]) is much larger than the hyperfine term (the second term on the right-hand side), which would result in a six-line spectrum for an isotropic resonance with $I = 5/2$.

In the $BaCeO_3$ crystal, eleven EPR absorption lines have been measured. The spacings between them are large enough and those between six principal absorption lines become wider with resonance magnetic field, which indicates that electron spin quantum number ($m_s$) and nuclear spin quantum number ($m_I$) are not good (pure) quantum numbers. We have to solve the Hamiltonian [1] exactly. The solution is well known (Breit–Rabi equation) and has been given by Ramsey (5) and others (6).

First, **I** and **S** are coupled together to form the resultant

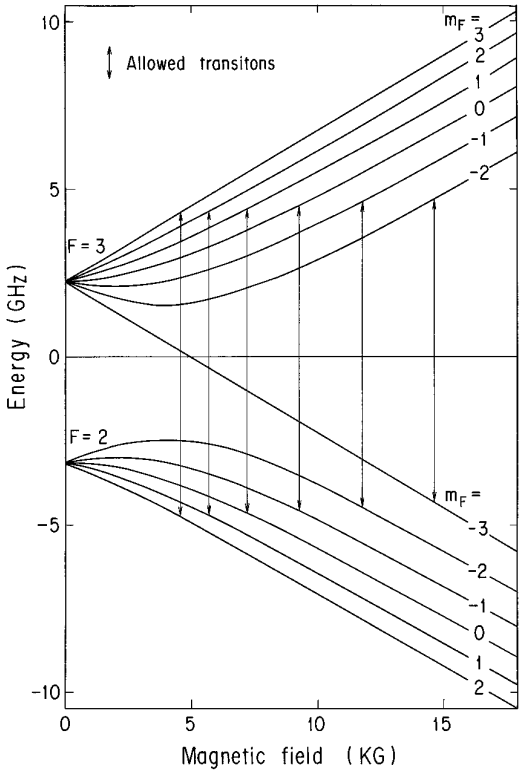


**FIG. 4.** Zeeman energy levels for $Pr^{4+}$ in $BaZrO_3$. Arrows show the observable EPR transitions at 4.2 K.

**F**, where $\mathbf{F} = \mathbf{I} + \mathbf{S}$. For $S = 1/2$ and $I = 5/2$ in the absence of a magnetic field, there are two states $F = 2$ and $F = 3$ which are separated by $3A$. When the magnetic field is included, each of these two states splits into $(2F + 1)\,|\,m_F\rangle$ Zeeman levels are shown in Fig. 4. Six allowed transitions ($\Delta F = \pm 1$; $\Delta m_F = \pm 1$) are observable. For $Pr^{4+}/BaCeO_3$ and $Pr^{4+}/BaCe_{0.90}Zr_{0.10}O_3$ five forbidden transitions ($\Delta F = \pm 1$; $\Delta m_F = 0$) are also observed.

The EPR spectra for $Pr^{4+}$ doped in the $BaSnO_3$ and

**TABLE 1**
**Experimental and Calculated EPR Absorption Line Positions for $BaPr_{0.02}Zr_{0.98}O_3$[a]**

| Experimental | Calculated[b] | Difference |
|---|---|---|
| — | 14,635 | |
| 11,746 | 11,745 | 1 |
| 9,254 | 9,261 | −7 |
| 7,254 | 7,251 | 3 |
| 5,724 | 5,717 | 7 |
| 4,592 | 4,588 | 4 |

[a] All values are given in $g$.
[b] Spin Hamiltonian parameters $|g| = 0.643$, $A = 0.0597$ cm$^{-1}$, $g_N$ set equal to 0.0.

**TABLE 2**
**Experimental and Calculated EPR Absorption Line Positions for $BaPr_{0.02}Sn_{0.98}O_3$[a]**

| Experimental | Calculated[b] | Difference |
|---|---|---|
| — | 16,078 | |
| 12,947 | 12,948 | −1 |
| 10,244 | 10,255 | −11 |
| 8,063 | 8,069 | −6 |
| 6,388 | 6,390 | −2 |
| 5,146 | 5,147 | −1 |

[a] All values are given in $g$.
[b] Spin Hamiltonian parameters $|g| = 0.583$, $A = 0.0589$ cm$^{-1}$, $g_N$ set equal to 0.0.

$BaZrO_3$ are broader than that doped in $BaCeO_3$ and the forbidden transitions are no longer observed in the former host materials. However, the number of the measured EPR absorption lines due to the hyperfine interaction with nuclear spin for $^{141}Pr$ ($I = 5/2$) is not six but five. To avoid incorrect assignments of the observed five absorption lines, we have prepared the samples for EPR measurements in which $Pr^{4+}$ ions are doped in $BaZr_yCe_{1-y}O_3$. The EPR spectra for $Pr^{4+}$ doped in $BaCeO_3$ have been previously assigned correctly and analyzed. With increasing Zr substitution for Ce (which corresponds to the shrinkage of the lattice), all the absorption lines move to higher field, which indicates that, in the EPR spectrum for $Pr^{4+}/BaZrO_3$, five allowed transitions have been observed and not the transition at the higher resonance field.

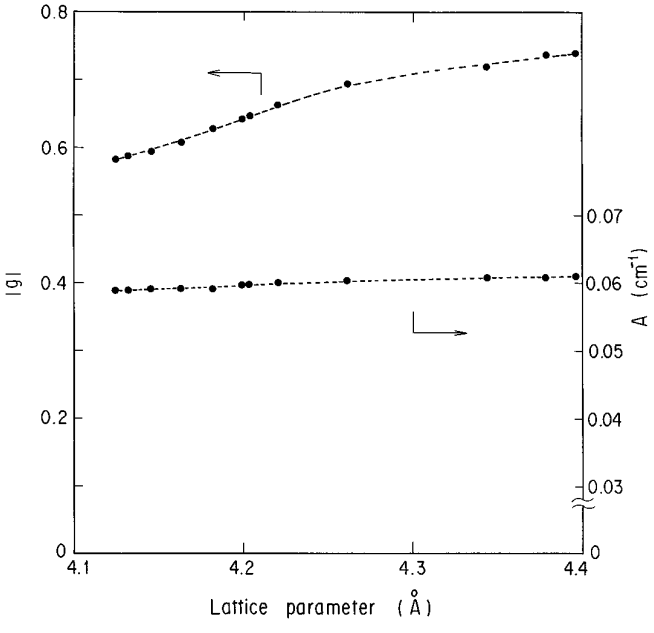


**FIG. 5.** $g$ value and $A$ vs lattice parameter for $Pr^{4+}$ in $BaMO_3$ ($M$ = Ce, Zr, Sn).

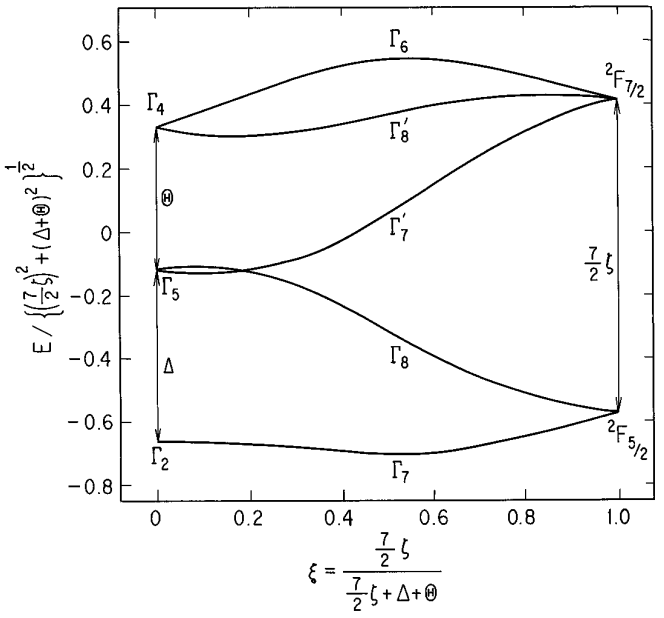


**FIG. 6.** Relative energy splittings of an $f^1$ electron as the relative magnitudes of the crystal field and spin–orbit coupling interactions change (octahedral symmetry).

The results of fitting the observed EPR spectra for $Pr^{4+}/BaZrO_3$ to the parameters of the spin Hamiltonian are shown in Table 1, with the best fit parameters $|g| = 0.643$ and $A = 0.0597$ cm$^{-1}$. The calculation results show that the resonance field for the sixth allowed transition is 14,635 G which is beyond our maximum magnetic field. Figure 4 shows the energy levels calculated for $Pr^{4+}$ in $BaZrO_3$. Arrows show the observable EPR transitions. With increasing Zr concentration in the host $BaZr_yCe_{1-y}O_3$, the EPR absorption line positions move to higher magnetic field. The same behavior has been found in the EPR spectra for $Pr^{4+}$ doped in $BaSn_yZr_{1-y}O_3$; i.e., with increasing Sn substitution for Zr (which means the shrinkage of lattice) the positions of the absorption lines move to higher magnetic field. The results of fitting the observed EPR spectra to the parameters of the spin Hamiltonian [1] are shown in Table 2, with the best fit parameters $|g| = 0.583$ and $A = 0.0589$ cm$^{-1}$. The resonance field for the sixth allowed transition is calculated to be 16,078 G.

Although the sign of the $g$ value is not obtained by this experiment, comparison with other $f^1$ systems in octahedral symmetry, such as $NpF_6/UF_6$ (7) and $Pa^{4+}/Cs_2ZrCl_6$ (6), where the sign of the $g$ value has been measured, indicates that the $g$ value for $Pr^{4+}/BaMO_3$ ($M$ = Ce, Zr, Sn) should be negative.

Figure 5 shows the $g$ value and hyperfine coupling constant $A$ against the lattice parameters for $BaCeO_3$, Ba(Ce,

**TABLE 3**
**Spin Hamiltonian Parameters and Crystal Field Splitting for $Pr^{4+}/BaMO_3$ ($M$ = Ce, Zr, Sn)**

| Host materials | Lattice parameter (Å) | $\|g\|$ | $A$ ($cm^{-1}$) | $\Delta$ ($cm^{-1}$) |
|---|---|---|---|---|
| $BaCeO_3$ | 4.3966[a] | 0.741 | 0.0609 | 1,693 |
| $BaCe_{0.90}Zr_{0.10}O_3$ | 4.3784[a] | 0.737 | 0.0608 | 1,701 |
| $BaCe_{0.70}Zr_{0.30}O_3$ | 4.3436 | 0.720 | 0.0607 | 1,734 |
| $BaCe_{0.30}Zr_{0.70}O_3$ | 4.2612 | 0.694 | 0.0604 | 1,784 |
| $BaCe_{0.10}Zr_{0.90}O_3$ | 4.2201 | 0.662 | 0.0600 | 1,846 |
| $BaZrO_3$ (Pr:5%) | 4.2034 | 0.648 | 0.0597 | 1,873 |
| $BaZrO_3$ (Pr:2%) | 4.1987 | 0.643 | 0.0597 | 1,883 |
| $BaSn_{0.25}Zr_{0.75}O_3$ | 4.1818 | 0.627 | 0.0592 | 1,914 |
| $BaSn_{0.50}Zr_{0.50}O_3$ | 4.1628 | 0.608 | 0.0593 | 1,951 |
| $BaSn_{0.75}Zr_{0.25}O_3$ | 4.1452 | 0.594 | 0.0590 | 1,978 |
| $BaSnO_3$ (Pr:5%) | 4.1311 | 0.587 | 0.0589 | 1,992 |
| $BaSnO_3$ (Pr:2%) | 4.1239 | 0.583 | 0.0589 | 1,996 |

[a] The actual lattice parameters for these orthorhombic $Pr^{4+}/BaCeO_3$ and $Pr^{4+}/BaCe_{0.90}Zr_{0.10}O_3$ are $a$ = 8.7931, $b$ = 6.2045, $c$ = 6.2248 Å and $a$ = 8.7559, $b$ = 6.1923, $c$ = 6.1923 Å, respectively. Since $a/2 \simeq b/\sqrt{2} \simeq c/\sqrt{2}$, the lattice parameters listed above are $a/2$.

Zr)$O_3$, $BaZrO_3$, Ba(Zr, Sn)$O_3$, and $BaSnO_3$ in which $Pr^{4+}$ ions are doped. With increasing size of the lattice, the value of $|g|$ increases. This result is in agreement with the discussion that the value of $|g|$ decreases with increasing crystal field strength as will be described below. On the other hand, the value of $A$ is almost constant, although a slight increase is found.

In the $BaMO_3$ ($M$ = Ce, Zr, Sn) host materials, the $Pr^{4+}$ ion is substituted for the $M^{4+}$ ion; i.e., it is in an octahedral site. The sevenfold orbitally degenerate energy state of the $f$ orbitals is split into a singlet state $\Gamma_2$ and two triplet states $\Gamma_4$ and $\Gamma_5$ in a strong crystal field (8). The energy difference between $\Gamma_2$ and $\Gamma_5$ is labeled as $\Delta$, and the energy difference between $\Gamma_4$ and $\Gamma_5$ is labeled as $\Theta$. This energy level splitting is shown on the left-hand side of Fig. 6.

When spin–orbit coupling is taken into account, (with $\zeta$ the spin–orbit coupling constant), the $\Gamma_2$ orbital state is transformed into a doublet $\Gamma_7$, and the $\Gamma_5$ and $\Gamma_4$ states are split into $\Gamma_7'$ (doublet) and $\Gamma_8$ (quartet), and $\Gamma_6$ (doublet) and $\Gamma_8'$ (quartet), respectively. The ordering of the levels is shown in Fig. 6. The $\Gamma_7$ level is lowest in energy. The energy matrices for the $\Gamma_7, \Gamma_8$, and $\Gamma_6$ states are

$$\Gamma_7: \begin{vmatrix} 0 & \sqrt{3}\zeta \\ \sqrt{3}\zeta & \Delta - \frac{1}{2}\zeta \end{vmatrix}$$

$$\Gamma_8: \begin{vmatrix} \Delta + \frac{1}{4}\zeta & \frac{3}{4}\sqrt{5}\zeta \\ \frac{3}{4}\sqrt{5}\zeta & \Delta + \Theta - \frac{3}{2}\zeta \end{vmatrix} \qquad [2]$$

$$\Gamma_6: |\Delta + \Theta + \tfrac{3}{2}\zeta|.$$

Diagonalization of the $\Gamma_7$ energy matrix gives the ground state $\Gamma_7$ and the excited state $\Gamma_7$, and the corresponding wavefunctions are written as

$$|\Gamma_7\rangle = \cos\theta|^2F_{5/2}, \Gamma_7\rangle - \sin\theta|^2F_{7/2}, \Gamma_7'\rangle, \qquad [3]$$

where $\theta$ is the parameter describing the admixture of the $\Gamma_7$ levels in the ground state, determined by the relation

$$\tan 2\theta = \frac{2\sqrt{3}\zeta}{\Delta - \frac{1}{2}\zeta}. \qquad [4]$$

The $g$ value for the ground state $\Gamma_7$ doublet is

$$g = 2\langle\Gamma_7|\mathbf{L} + 2\mathbf{S}|\Gamma_7\rangle = 2\cos^2\theta - \frac{4}{\sqrt{3}}\sin 2\theta. \qquad [5]$$

Using the $\Gamma_7$–$\Gamma_8$ splitting from Kern *et al.* (9) and the $g$ values given in this work and setting the spin–orbit coupling constant for $Pr^{4+}$ at its free ion value of 865 $cm^{-1}$ (10), we can determine the $\Delta$ and $\Theta$ values and calculate the energy levels. The data for $\Delta$ (which are sensitive to the crystal field strength) are collected in Table 3. With shrinkage of the lattice ($BaCeO_3 \rightarrow BaZrO_3 \rightarrow BaSnO_3$),

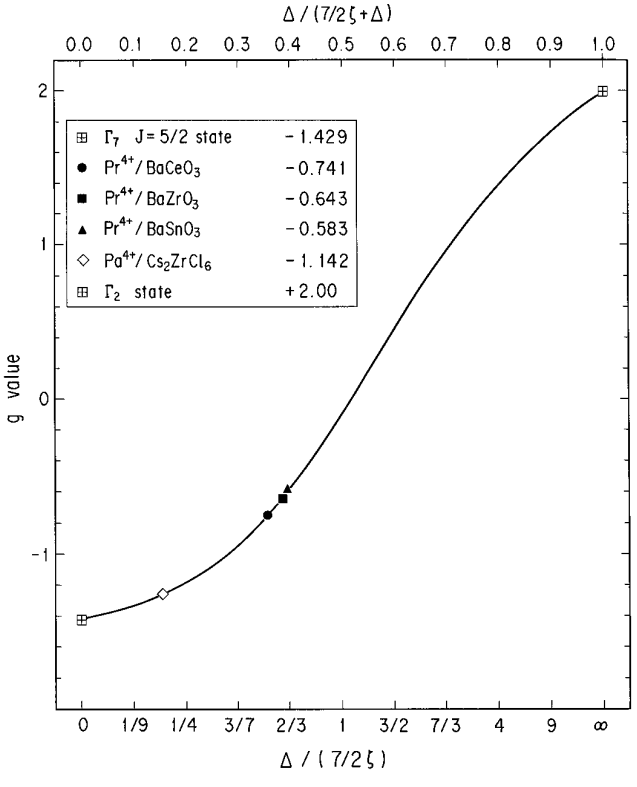


**FIG. 7.** $g$ value vs the ratio $\Delta/(7/2\zeta)$ for $Pr^{4+}$ in $BaMO_3$ ($M$ = Ce, Zr, Sn).

the $\Delta$ value (the energy difference between $\Gamma_2$ and $\Gamma_5$) increases. This is due to the increase of the crystal field strength by the shrinkage of the lattice.

The variation of the $g$ value against the $\Delta/(7/2\zeta)$ (ratio of the crystal field splitting to spin–orbit interaction) is shown in Fig. 7. This figure indicates that the crystal field strength is large in these compounds and that the effect of the crystal field in $Pr^{4+}/BaSnO_3$ is as large as that in $NpF_6/UF_6$ ($g = -0.608$).

## REFERENCES


1. N. E. Topp, "Chemistry of the Rare-Earth Elements." Elsevier, Amsterdam (1965).
2. J. B. Goodenough and J. M. Longo, *in* "Landolt-Börnstein Tabellen" (K.-H. Hellwege and A. M. Hellwege, Eds.), New Series, Vol. III, 4a, Chap. 3. Springer-Verlag, Berlin, 1970.
3. Y. Hinatsu and N. Edelstein, *J. Solid State Chem.* **112,** 53 (1994).
4. A. Abragam and B. Bleaney, "Electron Paramagnetic Resonance of Transition Ions" Chap. 5. Oxford Univ. Press, London, 1970.
5. N. F. Ramsey, "Molecular Beams." Clarendon Press, Oxford, 1956.
6. J. D. Axe, H. J. Stapleton, and C. D. Jeffries, *Phys. Rev.* **121,** 1630 (1961).
7. C. A. Hutchison and B. Weinstock, *J. Phys. Chem.* **32,** 56 (1960).
8. B. R. Judd, "Operator Techniques in Atomic Spectroscopy." McGraw-Hill, New York, 1963.
9. S. Kern, C.-K. Loong, and G. H. Lander, *Phys. Rev. B* **32,** 3051 (1985).
10. W. C. Martin, R. Zalubas, and L. Hagan, "Atomic Energy Levels—The Rare Earth Elements." NSRDS-NBS 60. U.S. Government Printing Office, Washington, DC, 1978.